THE JOURNAL OF PHYSICAL CHEMISTRY B
A JOURNAL OF THE AMERICAN CHEMICAL SOCIETY

pubs.acs.org/JPCB

Article

Methane Clathrate Formation is Catalyzed and Kinetically Inhibited by the Same Molecule: Two Facets of Methanol

Zhaoqian Su, Saman Alavi, John A. Ripmeester, Gedaliah Wolosh, and Cristiano L. Dias*

Cite This: *J. Phys. Chem. B* 2021, 125, 4162–4168

Read Online

ACCESS | Metrics & More | Article Recommendations | Supporting Information

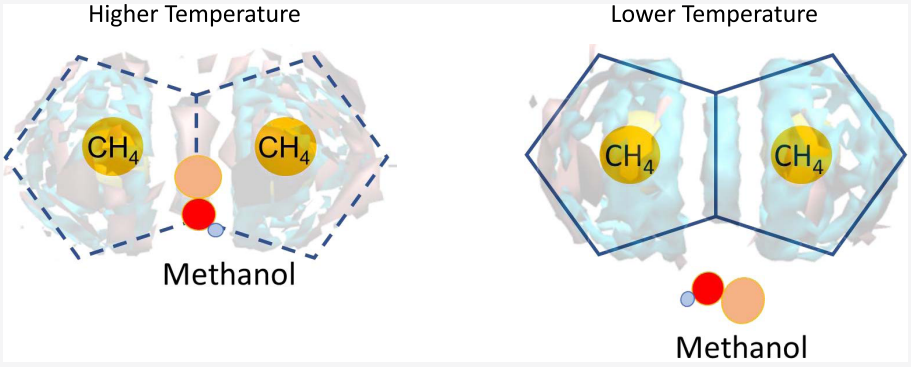

ABSTRACT: Here, we perform molecular dynamics simulations to provide atomic-level insights into the dual roles of methanol in enhancing and delaying the rate of methane clathrate hydrate nucleation. Consistent with experiments, we find that methanol slows clathrate hydrate nucleation above 250 K but promotes clathrate formation at temperatures below 250 K. We show that this behavior can be rationalized by the unusual temperature dependence of the methane−methanol interaction in an aqueous solution, which emerges due to the hydrophobic effect. In addition to its antifreeze properties at temperatures above 250 K, methanol competes with water to interact with methane prior to the formation of clathrate nuclei. Below 250 K, methanol encourages water to occupy the space between methane molecules favoring clathrate formation and it may additionally promote water mobility.

INTRODUCTION

Gas clathrate hydrates are solid inclusion compounds consisting of hydrogen-bonded water molecules encaging gas molecules.[1] They are naturally present under the seabed and in permafrost layers under low temperatures and high pressures favorable to the formation and stability of clathrate hydrates.[2−6] Due to the potential economical impact of extraction and synthesis of these structures, considerable efforts are being dedicated to control clathrate nucleation by the injection of small water-soluble molecules into the system.[5] In this process, some alcohols, particularly methanol, have been rediscovered to enhance the rate of clathrate hydrate nucleation at lower concentrations and very low temperatures, i.e., below 250 K.[7−13] This is surprising since at higher temperatures, alcohols are widely used to inhibit clathrate formation during the transport of natural gases in pipelines, thus avoiding plug formation.[1,14−17] Currently, the molecular mechanism of how the clathrate inhibition property of small alcohols is transformed into hydrate promoting behavior at lower temperatures is mostly unknown. We anticipate that filling this knowledge gap will not only contribute to a better understanding of clathrate formation but also enable the rational design of more efficient compounds to control this phenomenon.

Clathrate hydrates are space-filling cages consisting of hydrogen-bonded pentagonal and hexagonal water rings arranged around gas molecules. For methane hydrate, these cages are mostly pentagonal dodecahedra shown as 5^{12}, and tetradecahedra made of 2 hexagons and 12 pentagons, shown as $5^{12}6^2$.[18−20] Gas clathrate hydrates are formed from the packing of these polyhedra (or cages) into larger crystalline unit cells. One of the first hypotheses to explain clathrate nucleation was to consider a stepwise process in which individual cages form around gas molecules, followed by their diffusion in the solution and combination into larger aggregates.[21] However, computer simulations have found that individual cages are short-lived and disintegrate before forming aggregates.[22,23] It is now mostly accepted that homogeneous nucleation starts with the agglomeration of gas molecules into close proximity, triggering water to form cages in this

Received: February 10, 2021
Revised: March 31, 2021
Published: April 16, 2021

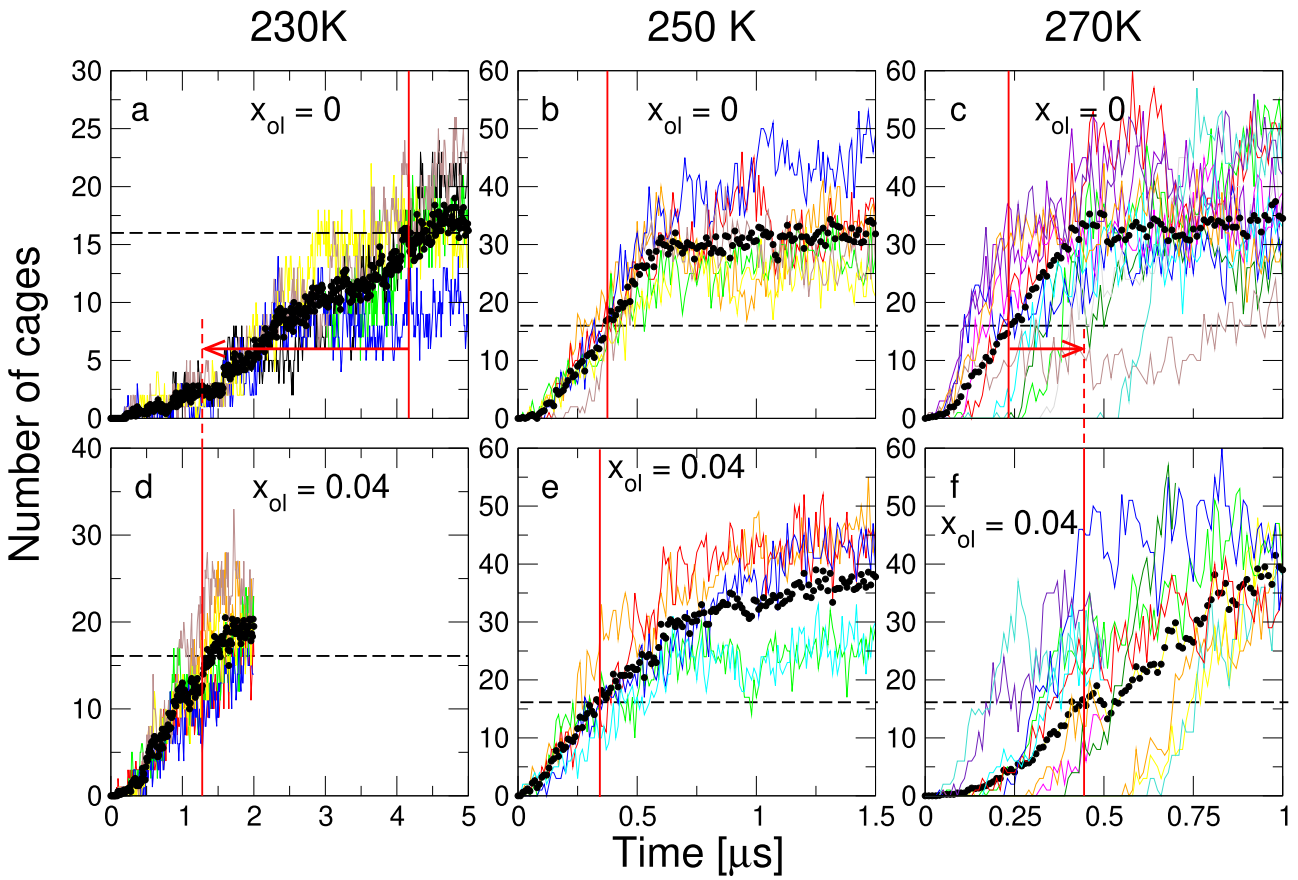

Figure 1. Measurement of nucleation of methane clathrates at 230 K (left panels), 250 K (middle panels), and 270 K (right panels) in solutions without methanol (upper panels) and methanol mole fraction x_{ol} = 0.04 (lower panels). Simulations performed using different initial conditions are represented by different colored lines. Black dots correspond to the average overall simulations performed under the same conditions of temperature, pressure, and methanol concentration. Red arrows show the effect of methanol on the time required to nucleate 16 methane.

space.[24,25] These cages are initially packed in amorphous structures and relax subsequently into a crystal.[26]

The antifreeze nature of alcohols is related to their effect on lowering the activity, and therefore decreasing the resulting thermodynamic chemical potential of the aqueous solution compared to the ice phase. This effect also partly accounts for their methane clathrate hydrate inhibiting property.[27−29] From a molecular point of view, this property of alcohols emerges from their disruption of the hydrogen-bond networks between water molecules in the liquid and their reduced capacity to form ordered hydrogen-bond structures.[30,31] However, recent X-ray diffraction and NMR experiments have shown that at low temperatures (253 K) and low concentrations, methanol plays a different role by increasing the rate of methane clathrate hydrate formation from ice−methanol mixtures exposed to pressures of methane gas.[8,10,11] At the same time, under these conditions, it is observed that limited amounts of methanol are incorporated into cages of the methane clathrate hydrate phase.[9] These recent studies suggest a complex role for methanol, wherein it can promote and inhibit gas clathrate hydrate formation depending on temperature and concentration.

Here, we perform molecular dynamics simulations to provide an atomic-level understanding of the complex role of methanol in the formation of methane clathrate. Consistent with experimental studies, we find that low concentrations of methanol promote clathrate formation at temperatures below ∼250 K but kinetically inhibit methane hydrate formation at temperatures above this value. Furthermore, isolated 5^{12} cages encapsulating methane molecules are found to be stabilized by methanol at temperatures below 250 K in the simulations. To rationalize these results, we study the interaction of methane dimers in water−methanol mixtures. We find that in aqueous solutions, methanol is attracted to methane at temperatures above 250 K. This dislodges water molecules from the vicinity of methane, which interferes with the formation of cages. In contrast, methanol is preferentially located away from methane at temperatures below 250 K, which enables water ordering and cage formation. We show that this temperature effect on the attraction of methanol to methane is driven by hydrophobic interactions between these molecules. Thus, in addition to the known effect of methanol in reducing the freezing point of water, our results show that methanol−methane interactions also play an important role in clathrate formation. This may have important implications for the design of new inhibitors since current efforts have focused mainly on how they affect the hydrogen-bond network of water (acting as thermodynamic inhibitors) or the surface of ice/clathrate structures (acting as kinetic inhibitors).[32,33]

SIMULATION METHODOLOGY

Simulations of cage formation and hydrate nucleation are performed using the TIP4P/ice model to represent water, a united-atom model is used for methane, and the OPLS model for methanol,[34−37] see Figure S1.[38] Given the low temperatures of the simulations, the internal degrees of freedom of the water,

https://doi.org/10.1021/acs.jpcb.1c01274
J. Phys. Chem. B 2021, 125, 4162−4168

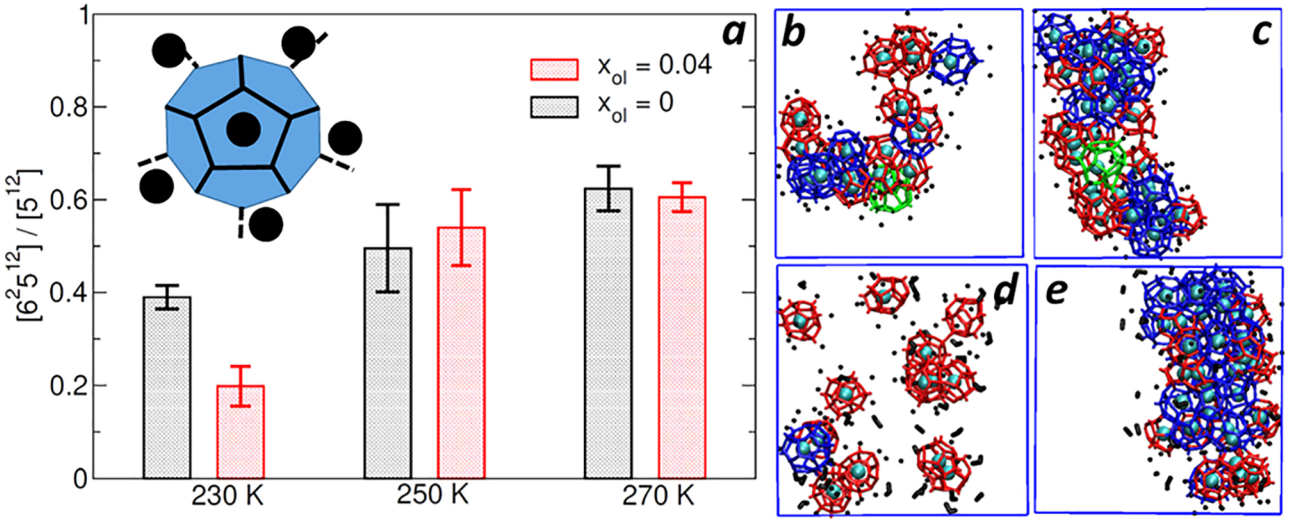

Figure 2. (a) Ratio of $5^{12}6^2$ to 5^{12} cages at different temperatures in the absence (black bars) and in the presence of a 0.04 mole fraction of methanol (red bars). Inset: Schematic representation of a 5^{12} cage encapsulating a methane molecule and surrounded by five methane molecules in the surrounding solution (black circles). Characteristic configurations of methane clathrates in pure water at (b) 230 K and (c) 270 K as well as in the presence of a 0.04 mole fraction of methanol at (d) 230 K and (e) 270 K. In these panels, methane molecules inside cages are shown using a van der Waals representation in cyan, whereas 5^{12}, $5^{12}6^2$, and $5^{12}6^4$ cages are represented in red, blue, and green, respectively. Methane and methanol molecules within 0.5 nm from cages are shown in licorice representation in black.

methane, and methanol molecules are not excited and the rigid molecule and united-atom potentials are adequate approximations for the simulations. These force fields reproduce the thermodynamic conditions of methane hydrate formation and phase coexistence properties of methanol over a wide range of temperatures.[39,40] Using these force fields, cages encapsulating methanol were shown to be stable in the methane hydrate phase at low temperatures.[41] Since the spontaneous nucleation of clathrates in computer simulation was found to occur for methane mole fractions (x_m) above 0.02−0.05 in water, we use x_m = 0.056 in all our simulations.[42,43] Notice that the equilibrium solubility of methane in water at hydrate conditions[44,45] is $x_m = 10^{-3}$ and, thus, much smaller than the one used in simulations. Accordingly, measured nucleation rates have been reported to be much smaller (10^{-7}−10^{-3} cm^{-3} s^{-1})[46,47] than the ones computed from molecular dynamics simulations (10^{23}−10^{26} cm^{-3} s^{-1}).[48] A total of 200 methane molecules are placed at random positions in the simulation box and the number of methanol/water molecules is chosen to account for the desired methane and methanol (x_{ol}) mole fractions. We perform more than five simulations using different initial configurations for each condition of temperature and x_{ol}, see Table S1.[38]

Simulations are performed in the NPT ensemble at a pressure of 50 MPa and temperatures below 304 K, which is the reported dissociation temperature of methane hydrate in computer simulations at 50 MPa.[49] The system is coupled to a velocity-rescaling thermostat (τ_T = 0.1 ps) to maintain a constant average temperature and the Parrinello−Rahman barostat (τ_P = 1 ps) is used to maintain an average pressure of 50 MPa. The particle-mesh Ewald (PME) method is used to treat long-range electrostatic interactions. A 1.0 nm cutoff distance is used for van der Waals interactions and short-range electrostatic interactions. Covalent bonds are constrained using the LINCS algorithm, and an integration time step of 2 fs is used together with the leap-frog integrator. Simulations are performed using GROMACS version 5.1[50] and open source software GRADE is used to compute the water cages in our simulations.[18] Umbrella sampling is also used to compute the potential of mean force (PMF) of methane dimers at different temperatures and x_{ol}. In these simulations, the distance ξ between methane molecules is used as the reaction coordinate and 25 windows are used to sample this distance up to 1.5 nm using springs with constant 4000 kJ mol^{-1} nm^{-2}. Equilibrium distances of springs at neighboring windows differ from each other by 0.05 nm with the smallest distance being 0.325 nm. Each window was simulated for 200 ns, see Table S2.[38] The weighted histogram analysis method (WHAM) is used to compute the PMF from simulations at different windows.[51]

RESULTS

Cage Formation. The number of cages formed in each simulation as a function of time is used to characterize the nucleation process. In Figure 1, the total number of cages (i.e., 5^{12}, $5^{12}6^2$, and $5^{12}6^4$) formed in the absence and the presence of methanol at x_{ol} = 0.04 and three temperatures is shown as a function of time. At least five trajectories are shown for each temperature and methanol mole fraction with different colored thin lines. The average number of cages formed from these trajectories as a function of time is shown using the black dots. The total number of cages formed increases continuously from zero and converges to different values for the different simulation conditions. The vertical red lines depict the time required for the average number of cages to reach 16. This number was chosen arbitrarily as a gauge of the nucleation process to enable comparison between different simulations. In the absence of methanol at 230, 250, and 270 K (Figure 1a−c), approximately 4.2, 0.37, and 0.24 μs are required for 16 cages to form, respectively. Thus, increasing temperature speeds up the formation of clathrates. It should be noted that the low methanol concentration of x_{ol} = 0.04 in the aqueous solution is in the range that allows for kinetic inhibition or kinetic enhancement of hydrate formation for methanol, while still allowing the formation of the methane hydrate phase over long times. Higher methanol concentrations in the aqueous phase would be needed for the thermodynamic inhibition effect of

https://doi.org/10.1021/acs.jpcb.1c01274
J. Phys. Chem. B 2021, 125, 4162−4168

methanol to come into effect and to prevent the complete formation of a methane hydrate phase. As shown in Figure 1, the number of cages formed in the system, methane hydrate nucleation, and hydrate phase growth occur to different extents for the 1 μs duration of each simulation, based on the thermodynamic conditions of the simulation.

The addition of methanol to the solution affects the time required for clathrates to form in a temperature-dependent manner. At 270 K, the time required for 16 cages to form increases from 0.24 to 0.45 μs when methanol molecules are added to the solution, see the red arrow in Figure 1c. This is consistent with the well-known effect of methanol, which is to inhibit the formation of ice and gas clathrates by disrupting the water hydrogen-bonding network.[32] At 250 K, the time required to form 16 cages does not change significantly when methanol is added to the solution. Surprisingly, the addition of methanol to the solution at 230 K reduces the cage formation time to approximately 1.3 μs from 4.2 μs, see the arrow in Figure 1a. Thus, methanol increases the rate of clathrate formation at very low temperatures (230 K) but decreases the rate at close to ice freezing temperatures (270 K).

In Figure 2, we analyze the types of clathrates formed in our simulations. Most of the cages are of the $5^{12}6^2$ and the 5^{12} types and the ratio of the former to the latter averaged over the last 100 ns is shown in Figure 2a.[37] In the absence of methanol, this ratio decreases with decreasing temperature from 0.6 at 270 K to 0.4 at 230 K. Methanol only affects the ratio of $5^{12}6^2$ to 5^{12} cages in a significant manner at 230 K. At this temperature, the ratio decreases from 0.4 to 0.2 when methanol is added to the solution. Figure 2b–e shows snapshots of the final configurations of a characteristic simulation performed at 230 and 270 K in the absence and the presence of methanol. At 270 K, cages are tightly packed, both in the absence (Figure 2c) and the presence (Figure 2e) of methanol whereas, at 230 K, they are more isolated and exposed to the solvent. The latter phenomenon is particularly pronounced in the presence of methanol (Figure 2d), wherein several isolate 5^{12} cages are found stable in our simulations. These differences in cage packing are further highlighted in Figures S4 and S5, where the last configurations of six simulations at high (270 K) and low (230 K) temperatures in the presence of methanol are shown.

Cluster Analysis. To investigate how cage packing evolves during the simulation, we depict in Figure 3 results from cluster analysis. Here, we use the position of guest molecules to compute distances between cages, and we consider that a cage is a part of a cluster if its distance to any cage belonging to that cluster is less than 0.85 nm.[37] This cutoff distance to measure clusters is used since guest molecules are at an approximate distance of 0.7 nm from each other in first-neighbor cages. Figure 3 shows the time dependence of both the largest cluster size (in red) and the fraction f_c of cages forming the largest cluster (in black). The largest cluster size is defined in terms of the number of cages that it comprises and f_c corresponds to this number divided by the total number of cages in the simulation box. We report the average of these quantities over the different simulations. In all simulations, the size of the largest cluster grows as a function of time. At 270 K, the largest cluster contains most of the cages in the box (panels b and d) as f_c is close to one at all times. This is consistent with an image in which cages are stable when at close proximity from other cages but short-lived when isolated in the simulation box. In

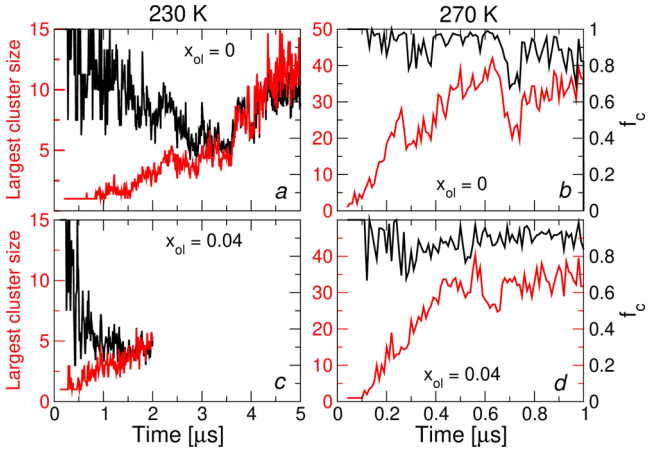

Figure 3. Cluster analysis of simulations performed at 230 and 270 K in the presence and the absence of methanol. The largest cluster size (in red) and the fraction of cages f_c that belongs to the largest cluster (in black) averaged over the different simulations are shown as a function of time. The same scale is used to represent f_c in all four panels.

the absence of methanol at 230 K (panel a), f_c decreases in the first 3 μs implying that, in this time interval, most of the new cages formed are not in contact with the largest cluster. After 3 μs, the growth of the largest cluster dominates over the formation of isolated cages, which leads to an increase in f_c. At the end of the simulation when 17 cages are present in the simulation box, most cages are part of the largest cluster as $f_c \sim 0.7$. In contrast to this result, in the presence of methanol at 230 K (panel c), f_c decreases, reaching a value of 0.3 at the end of the simulation when the same number of cages are present in the simulation box. This implies that the presence of small clusters is more pronounced in a methanol solution.

Notice that the difference in the spatial distribution of cages at 230 K occurs despite its total number being approximately the same (i.e., ~17) in the presence and the absence of methanol at the end of simulations, see Figure 1. These 17 cages were formed in only 2 μs in simulations with methanol and 5 μs in pure water, highlighting a significant role of methanol in promoting clathrate formation. One factor that could contribute to this high rate of formation is the ability of methanol to behave as a guest molecule for $5^{12}6^2$ and $5^{12}6^4$ cages due to its small size. For example, in Figure S5, we show two cages at 270 K for which methanol is the guest molecule. However, methanol was not the guest of any cages in our simulations at 230 K, suggesting that, at this low temperature, its main role is in promoting methane cages.

Computational studies have shown that the formation of clathrates in pure water starts with the agglomeration of methane molecules into specific configurations wherein they are separated from each other by one layer of water.[24,26,52] These are known as solvent-separated configurations (SSC). The inset of Figure 2a shows a schematic representation of SSC supporting a 5^{12} cage. In this configuration, methane inside and outside the cage is separated by one layer of water molecules. In Figure 2b–e, SSC is illustrated by depicting methane and methanol (in black) that are 0.5 nm apart from cages. The greater exposure of cages to the solvent at 230 K accounts for a larger number of methane/methanol surrounding cages (Figure 2d). Effects of methanol on SSC may provide some insights into its catalytic effect on methane clathrate

https://doi.org/10.1021/acs.jpcb.1c01274
J. Phys. Chem. B 2021, 125, 4162–4168

formation at low temperatures. Thus, we study next how methanol affects the energy of SSC configuration.

Potential of Mean Force. To investigate the effect of methanol on the stability of SSC, we show in Figure 4, the potential of mean force (PMF) of methane dimers computed in the presence and the absence of methanol at different temperatures. These PMFs are a function of the distance ξ between methane molecules and they correspond to the free energy required to bring these molecules from distances where they are not interacting with each other ($\geq$1.5 nm) to ξ.[53−55] The PMF is normalized to zero at large distances. The first minimum of the PMF, which occurs at ξ_{cm} = 0.38 nm corresponds to contact configurations (CC) in which methane molecules are in contact with each other. The second minimum of the PMF (at ∼0.7 nm) corresponds to SSC, where a layer of water separates the two methane molecules. The desolvation barrier (db) in between CC and SSC is associated with the free-energy cost of removing water from the space between methane molecules as they are brought together.

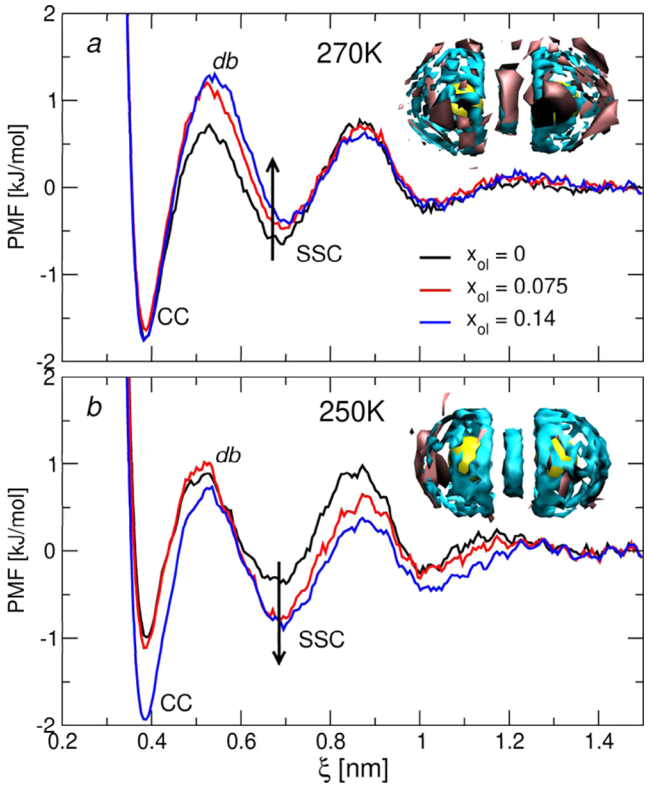

Figure 4. Potential of mean force (PMF) of a methane dimer in pure water (black) and methanol solutions (red and blue) at 270 K (upper panel) and 250 K (lower panel). PMF values computed at ξ = 1.45 nm are used as our reference, i.e., zero value. Insets depict the spatial distribution functions of methanol (pink color) and water (cyan color) around a methane dimer (in yellow) in solutions containing a methanol mole fraction of 0.075. The probability isovalues for methanol and water in the spatial distribution functions are 8.4 and 0.57, respectively.

At 270 K, the PMF associated with SSC and db configurations increases in magnitude with increasing methanol concentration, see Figure 4a. In contrast, at 230 K, the PMF at SSC decreases in magnitude with increasing methanol concentration, and at a high mole fraction (x_{ol} = 0.14), the PMF at CC is also significantly lower, see Figure 4b. Thus, methanol discourages and favors the formation of SSC at 270 and 250 K. The latter causes an increased presence of SSC in the simulation box, which is expected to facilitate clathrate nucleation and may lead to a reduced time of formation, as reported in Figure 1. Notice that simulations of methane dimers were not performed at 230 K due to rapid freezing of the system, which makes it challenging to sample the conformational space required to compute the PMF.

To rationalize these results, the inset of Figure 4 depicts the spatial distribution of water (in cyan) and methanol (in pink) around methane dimers (yellow spheres) computed at SSC. There is a significant probability of observing methanol molecules in the space between the two methane at 270 K, whereas, at 250 K, only water occupies this space. This suggests competition between methanol and water for the space between methane dimers at 270 K, which contribute to destabilizing cages. In other words, water molecules, which form a network of hydrogen bonds that stabilizes the formation of SSC, are being dislodged by methanol. In contrast, at 250 K, methane is mostly surrounded by water molecules (see the inset) with methanol being located preferentially away from the dimer. Hydrophobic interactions between methyl groups of methanol ($-CH_3$) and methane (CH_4) constitute a possible mechanism for the enhanced attraction of these molecules with increasing temperature.[56,57] In Section S3 of the Supporting Information, we compute methane−methanol radial distribution functions from our methane-dimer simulations at 250 and 270 K, see Figure S2.[38] These quantities are used to decompose the methane−methanol PMF at 250 K into its entropic and enthalpic components, see Figure S3.[38] This shows that methane−methanol interactions are dominated by entropy, which is consistent with the nature of the hydrophobic effect.[53,58,59]

Methanol may also have a secondary effect on the rate of hydrate nucleation and formation by leading to an increase in the mobility of water at low temperatures, which would contribute to its catalytic role. This was demonstrated in experiments and simulations in which hydrates are formed by vapor deposition of gases onto amorphous ice phases.[8] To quantify this effect of methanol, we measure the diffusion coefficients of water molecules in the simulations shown in Figure 1. In the absence of methanol and at 270 K, the water diffusion coefficient is 152 $\mu m^2\ s^{-1}$, which is much smaller than the one measured experimentally for pure liquid water at 273 K, which is 1050 $\mu m^2\ s^{-1}$.[60] This difference is anticipated as several water molecules are partially immobilized around cages in our simulations. In the presence of methanol, binding of water molecules to this alcohol accounts for a small reduction of the diffusion coefficient to 115 $\mu m^2\ s^{-1}$. At 230 K, the diffusion coefficient of water is 2.1 $\mu m^2\ s^{-1}$ and, in the presence of methanol, it undergoes a small increase to 2.4 $\mu m^2\ s^{-1}$. This small increase in the diffusion coefficient may not be the main factor accounting for the speed up in clathrate formation observed in Figure 1a,d but it can contribute to increased mobility of water molecules, enabling rearrangement into hydrate cages.

CONCLUSIONS

In summary, we have performed extensive molecular dynamics simulations to provide insights into the mechanisms accounting for the ambivalent effects of methanol on clathrate formation. In addition to the antifreeze property of methanol,

https://doi.org/10.1021/acs.jpcb.1c01274
J. Phys. Chem. B 2021, 125, 4162−4168

we find that at temperatures above 250 K, this alcohol is attracted to the vicinity of methane molecules. This dislodges water molecules from the neighborhood of methane, which are required for the formation of cages discouraging clathrate nucleation. Below 250 K, methanol is preferentially located away from methane molecules, enabling water molecules to stabilize SSC that support the formation of cages. Accordingly, below 250 K and in the presence of methanol, small clusters of cages are found to be stable in our simulations, suggesting that, at these low temperatures, clathrate formation may proceed through the diffusion and aggregation of these units. The temperature-dependent attraction of methanol and methane is accounted for by hydrophobic interactions, which are entropic in nature and increase in the magnitude with increasing temperature. Moreover, at very low temperatures, methanol accounts for a small increase in the diffusion coefficient of water, which may contribute to the faster formation of clathrates.

■ ASSOCIATED CONTENT

Supporting Information

The Supporting Information is available free of charge at https://pubs.acs.org/doi/10.1021/acs.jpcb.1c01274.

Additional information about force-field parameters, simulation setup, methane−methanol interactions, and cage packing in the presence of methanol (PDF)

■ AUTHOR INFORMATION

Corresponding Author

Cristiano L. Dias − *New Jersey Institute of Technology, Department of Physics, University Heights, Newark, New Jersey 07102, United States;* orcid.org/0000-0002-8765-3922; Email: cld@njit.edu

Authors

Zhaoqian Su − *Department of Systems and Computational Biology, Albert Einstein College of Medicine, Bronx, New York 10461, United States;* orcid.org/0000-0002-8369-0697

Saman Alavi − *Department of Chemistry and Biomolecular Sciences, University of Ottawa, Ottawa, Ontario K1N 6N5, Canada;* orcid.org/0000-0001-9463-8766

John A. Ripmeester − *National Research Council of Canada, Ottawa, Ontario K1A 0R6, Canada;* orcid.org/0000-0002-4091-5120

Gedaliah Wolosh − *New Jersey Institute of Technology, Academic and Research Computing Systems, University Heights, Newark, New Jersey 07102, United States*

Complete contact information is available at: https://pubs.acs.org/10.1021/acs.jpcb.1c01274

Notes

The authors declare no competing financial interest.

■ ACKNOWLEDGMENTS

This work was financially supported through a grant from the ACS-PRF#58024ND6 to C.L.D. Computational resources for this work were provided by the Academic and Research Computing Systems at the New Jersey Institute of Technology.

■ REFERENCES

(1) Sloan, E. D., Jr.; Koh, C. A. *Clathrate Hydrates of Natural Gases*; CRC Press, 2007.

(2) Grace, J.; Collett, T.; Colwell, F.; Englezos, P.; Jones, E.; Mansell, R.; Meekison, J.; Ommer, R.; Pooladi-Darvish, M.; Riedel, M. et al. *Energy from Gas Hydrates—Assessing the Opportunities and Challenges for Canada*; Council of Canadian Academies, 2008.

(3) Sum, A. K.; Koh, C. A.; Sloan, E. D. Clathrate hydrates: from laboratory science to engineering practice. *Ind. Eng. Chem. Res.* **2009**, *48*, 7457−7465.

(4) Sloan, E. D. Fundamental principles and applications of natural gas hydrates. *Nature* **2003**, *426*, 353−363.

(5) Englezos, P.; Lee, J. D. Gas hydrates: A cleaner source of energy and opportunity for innovative technologies. *Korean J. Chem. Eng.* **2005**, *22*, 671−681.

(6) Koh, C. A.; Sum, A. K.; Sloan, E. D. Gas hydrates: Unlocking the energy from icy cages. *J. Appl. Phys.* **2009**, *106*, No. 061101.

(7) Blake, D.; Allamandola, L.; Sandford, S.; Hudgins, D.; Freund, F. Clathrate hydrate formation in amorphous cometary ice analogs in vacuo. *Science* **1991**, *254*, 548−551.

(8) McLaurin, G.; Shin, K.; Alavi, S.; Ripmeester, J. A. Antifreezes Act as Catalysts for Methane Hydrate Formation from Ice. *Angew. Chem.* **2014**, *126*, 10597−10601.

(9) Shin, K.; Udachin, K. A.; Moudrakovski, I. L.; Leek, D. M.; Alavi, S.; Ratcliffe, C. I.; Ripmeester, J. A. Methanol incorporation in clathrate hydrates and the implications for oil and gas pipeline flow assurance and icy planetary bodies. *Proc. Natl. Acad. Sci. U.S.A.* **2013**, *110*, 8437−8442.

(10) Abay, H. K.; Svartaas, T. M. Effect of ultralow concentration of methanol on methane hydrate formation. *Energy Fuels* **2010**, *24*, 752−757.

(11) Ke, W.; Svartaas, T. M.; Abay, H. K. Effects of low concentration methanol, PVP and PVCap on Structure-I methane hydrate formation. *J. Energy Power Eng.* **2013**, *7*, 432.

(12) Devlin, J. P. Catalytic activity of methanol in all-vapor subsecond clathrate-hydrate formation. *J. Chem. Phys.* **2014**, *140*, No. 164505.

(13) Bobev, S.; Tait, K. T. Methanol-inhibitor or promoter of the formation of gas hydrates from deuterated ice? *Am. Mineral.* **2004**, *89*, 1208−1214.

(14) Hammerschmidt, E. Formation of gas hydrates in natural gas transmission lines. *Ind. Eng. Chem.* **1934**, *26*, 851−855.

(15) Østergaard, K. K.; Masoudi, R.; Tohidi, B.; Danesh, A.; Todd, A. C. A general correlation for predicting the suppression of hydrate dissociation temperature in the presence of thermodynamic inhibitors. *J. Pet. Sci. Eng.* **2005**, *48*, 70−80.

(16) Robinson, D. Hydrate formation and inhibition in gas or gas condensate streams. *J. Can. Pet. Technol.* **1986**, *25*, 26−30.

(17) Ng, H.-J.; Robinson, D. B. Hydrate formation in systems containing methane, ethane, propane, carbon dioxide or hydrogen sulfide in the presence of methanol. *Fluid Phase Equilib.* **1985**, *21*, 145−155.

(18) Mahmoudinobar, F.; Dias, C. L. GRADE: A code to determine clathrate hydrate structures. *Comput. Phys. Commun.* **2019**, *244*, 385−391.

(19) Nguyen, A. H.; Molinero, V. Identification of clathrate hydrates, hexagonal ice, cubic ice, and liquid water in simulations: The CHILL+ algorithm. *J. Phys. Chem. B* **2015**, *119*, 9369−9376.

(20) Jacobson, L. C.; Hujo, W.; Molinero, V. Thermodynamic stability and growth of guest-free clathrate hydrates: a low-density crystal phase of water. *J. Phys. Chem. B* **2009**, *113*, 10298−10307.

(21) Christiansen, R. L.; Sloan, E. D. Mechanisms and kinetics of hydrate formation. *Ann. N. Y. Acad. Sci.* **1994**, *715*, 283−305.

(22) Guo, G.-J.; Zhang, Y.-G.; Zhao, Y.-J.; Refson, K.; Shan, G.-H. Lifetimes of cagelike water clusters immersed in bulk liquid water: A molecular dynamics study on gas hydrate nucleation mechanisms. *J. Chem. Phys.* **2004**, *121*, 1542.

(23) Guo, G.-J.; Zhang, Y.-G.; Liu, H. Effect of methane adsorption on the lifetime of a dodecahedral water cluster immersed in liquid

water: A molecular dynamics study on the hydrate nucleation mechanisms. *J. Phys. Chem. C* **2007**, *111*, 2595−2606.
(24) Walsh, M. R.; Koh, C. A.; Sloan, E. D.; Sum, A. K.; Wu, D. T. Microsecond simulations of spontaneous methane hydrate nucleation and growth. *Science* **2009**, *326*, 1095−1098.
(25) Radhakrishnan, R.; Trout, B. L. A new approach for studying nucleation phenomena using molecular simulations: Application to CO2 hydrate clathrates. *J. Chem. Phys.* **2002**, *117*, 1786−1796.
(26) Jacobson, L. C.; Hujo, W.; Molinero, V. Amorphous precursors in the nucleation of clathrate hydrates. *J. Am. Chem. Soc.* **2010**, *132*, 11806−11811.
(27) Deschamps, F.; Mousis, O.; Sanchez-Valle, C.; Lunine, J. I. The role of methanol in the crystallization of Titan's primordial ocean. *Astrophys. J.* **2010**, *724*, 887−894.
(28) Miller, G. A.; Carpenter, D. K. Solid-Liquid Phase Diagram of the System Methanol-Water. *J. Chem. Eng. Data* **1964**, *9*, 371−373.
(29) Pascal, T. A.; III, W. A. G. Hydrophobic Segregation, Phase Transitions and the Anomalous Thermodynamics of Water/Methanol Mixtures. *J. Phys. Chem. B* **2012**, *116*, 13905−13912.
(30) Israelachvili, J. N. *Intermolecular and Surface Forces*; Academic Press, 2011.
(31) Bakó, I.; Megyes, T.; Bálint, S.; Groósza, T.; Chihaia, V. Water-methanol mixtures: topology of hydrogen bonded network. *Phys. Chem. Chem. Phys.* **2008**, *10*, 5004−5011.
(32) Yagasaki, T.; Matsumoto, M.; Tanaka, H. Effects of thermodynamic inhibitors on the dissociation of methane hydrate: a molecular dynamics study. *Phys. Chem. Chem. Phys.* **2015**, *17*, 32347−32357.
(33) Anderson, B. J.; Tester, J. W.; Borghi, G. P.; Trout, B. L. Properties of inhibitors of methane hydrate formation via molecular dynamics simulations. *J. Am. Chem. Soc.* **2005**, *127*, 17852−17862.
(34) Abascal, J.; Sanz, E.; Fernández, R. G.; Vega, C. A potential model for the study of ices and amorphous water: TIP4P/Ice. *J. Chem. Phys.* **2005**, *122*, No. 234511.
(35) Martin, M. G.; Siepmann, J. I. Transferable potentials for phase equilibria. 1. United-atom description of n-alkanes. *J. Phys. Chem. B* **1998**, *102*, 2569−2577.
(36) van Leeuwen, M. E.; Smit, B. Molecular simulation of the vapor-liquid coexistence curve of methanol. *J. Phys. Chem. A* **1995**, *99*, 1831−1833.
(37) Sarupria, S.; Debenedetti, P. G. Homogeneous nucleation of methane hydrate in microsecond molecular dynamics simulations. *J. Phys. Chem. Lett.* **2012**, *3*, 2942−2947.
(38) See Supplemental Material at [URL will be inserted by publisher] for [give brief description of material].
(39) Conde, M. M.; Rovere, M.; Gallo, P. High precision determination of the melting points of water TIP4P/2005 and TIP4P/Ice models by direct coexistance technique. *J. Chem. Phys.* **2017**, *147*, No. 244506.
(40) Gonzalez-Salgado, D.; Dopazo-Paz, A.; Gomez-Alvarez, P.; Miguez, J. M.; Vega, C. Solid-Solid and Solid-Fluid Equilibria of the Most Popular Models of Methanol Obtained by Computer Simulation. *J. Phys. Chem. B* **2011**, *115*, 3522−3530.
(41) Alavi, S.; Shin, K.; Ripmeester, J. A. Molecular Dynamics Simulations of Hydrogen Bonding in Clathrate Hydrates with Ammonia and Methanol Guest Molecules. *J. Chem. Eng. Data* **2015**, *60*, 389−397.
(42) Walsh, M. R.; Beckham, G. T.; Koh, C. A.; Sloan, E. D.; Wu, D. T.; Sum, A. K. Methane Hydrate Nucleation Rates from Molecular Dynamics Simulations: Effects of Aqueous Methane Concentration, Interfacial Curvature, and System Size. *J. Phys. Chem. C* **2011**, *115*, 21241−21248.
(43) Guo, G.-J.; Rodger, P. M. Solubility of Aqueous Methane under Metastable Conditions: Implications for Gas Hydrate Nucleation. *J. Phys. Chem. B* **2013**, *117*, 6498−6504.
(44) Kim, Y.; Ryu, S.; Yang, S.; Lee, C. Liquid water-hydrate equilibrium measurements and unified predictions of hydrate-containing phase equilibria for methane, ethane, propane, and their mixtures. *Ind. Eng. Chem. Res.* **2003**, *42*, 2409−2414.
(45) Servio, P.; Englezos, P. Measurement of dissolved methane in water in equilibrium with its hydrate. *J. Chem. Eng. Data* **2002**, *47*, 87−90.
(46) Devarakonda, S.; Groysman, A.; Myerson, A. S. THF-water hydrate crystallization: an experimental investigation. *J. Cryst. Growth* **1999**, *204*, 525−538.
(47) Abay, H. K.; Svartaas, T. M. Multicomponent gas hydrate nucleation: the effect of the cooling rate and composition. *Energy Fuels* **2011**, *25*, 42−51.
(48) Barnes, B. C.; Knott, B. C.; Beckham, G. T.; Wu, D. T.; Sum, A. K. Reaction coordinate of incipient methane clathrate hydrate nucleation. *J. Phys. Chem. B* **2014**, *118*, 13236−13243.
(49) Conde, M.; Vega, C. Determining the three-phase coexistence line in methane hydrates using computer simulations. *J. Chem. Phys.* **2010**, *133*, No. 064507.
(50) van der Spoel, D.; Lindahl, E.; Hess, B.; Groenhof, G.; Mark, A. E.; Berendsen, H. J. GROMACS: fast, flexible, and free. *J. Comput. Chem.* **2005**, *26*, 1701−1718.
(51) Hub, J. S.; de Groot, B. L.; Van Der Spoel, D. g_wham-A Free Weighted Histogram Analysis Implementation Including Robust Error and Autocorrelation Estimates. *J. Chem. Theory Comput.* **2010**, *6*, 3713−3720.
(52) Debenedetti, P. G.; Sarupria, S. Hydrate molecular ballet. *Science* **2009**, *326*, 1070−1071.
(53) Southall, N. T.; Dill, K. A. Potential of mean force between two hydrophobic solutes in water. *Biophys. Chem.* **2002**, *101−102*, 295−307.
(54) Dias, C. L.; Chan, H. S. Pressure-dependent properties of elementary hydrophobic interactions: ramifications for activation properties of protein folding. *J. Phys. Chem. B* **2014**, *118*, 7488−7509.
(55) Pratt, L. R.; Chandler, D. Theory of the hydrophobic effect. *J. Chem. Phys.* **1977**, *67*, 3683.
(56) Dias, C. L.; Ala-Nissila, T.; Wong-ekkabut, J.; Vattulainen, I.; Grant, M.; Karttunen, M. The hydrophobic effect and its role in cold denaturation. *Cryobiology* **2010**, *60*, 91−99.
(57) Kauzmann, W. Factors in interpretation of protein denaturation. *Adv. Protein Chem.* **1959**, *14*, 1.
(58) Dias, C. L.; Hynninen, T.; Ala-Nissila, T.; Foster, A. S.; Karttunen, M. Hydrophobicity within the three-dimensional Mercedes-Benz model: Potential of mean force. *J. Chem. Phys.* **2011**, *134*, No. 065106.
(59) Dill, K. A. Dominant Forces in Protein Folding. *Biochemistry* **1990**, *29*, 7133.
(60) Gillen, K. T.; Douglass, D.; Hoch, M. Self-diffusion in liquid water to- 31 C. *J. Chem. Phys.* **1972**, *57*, 5117−5119.

https://doi.org/10.1021/acs.jpcb.1c01274
J. Phys. Chem. B 2021, 125, 4162−4168